Na^+-TRANSLOCATING MEMBRANE PYROPHOSPHATASES ARE WIDESPREAD IN THE MICROBIAL WORLD AND EVOLUTIONARILY PRECEDE H^+-TRANSLOCATING PYROPHOSPHATASES*

Heidi Luoto[‡], Georgiy A. Belogurov[‡], Alexander A. Baykov[§], Reijo Lahti[‡], and Anssi M. Malinen[‡1]

From the [‡]Department of Biochemistry and Food Chemisty, University of Turku, FIN-20014 Turku, Finland, and the [§]A. N. Belozersky Institute of Physico-Chemical Biology, Moscow State University, Moscow 119899, Russia

Running head: Transport specificity of membrane pyrophosphatases

[1]Address correspondence to: Anssi Malinen, Department of Biochemistry and Food Chemistry, Vatselankatu 2, 20014 University of Turku, Turku, Finland. Tel. +35823336855, Fax: +35823336860, E-mail: anssi.malinen@utu.fi

Membrane pyrophosphatases (PPases), divided into K^+-dependent and K^+-independent subfamilies, were believed to pump H^+ across cell membranes until a recent demonstration that some K^+-dependent PPases function as Na^+ pumps. Here, we have expressed seven evolutionarily important putative PPases in *Escherichia coli* and estimated their hydrolytic, Na^+ transport and H^+ transport activities as well as their K^+ and Na^+ requirements in inner membrane vesicles. Four of these enzymes (from *Anaerostipes caccae*, *Chlorobium limicola*, *Clostridium tetani* and *Desulfuromonas acetoxidans*) were identified as K^+-dependent Na^+ transporters. Phylogenetic analysis led to the identification of a monophyletic clade comprising characterized and predicted Na^+-transporting PPases (Na^+-PPases) within the K^+-dependent subfamily. H^+-transporting PPases (H^+-PPases) are more heterogeneous and form at least three independent clades in both subfamilies. These results suggest that rather than being a curious rarity, Na^+-transporting PPases predominantly constitute the K^+-dependent subfamily. Furthermore, Na^+-PPases possibly precede H^+-PPases in evolution, and transition from Na^+ to H^+ transport may have occurred in several independent enzyme lineages. Site-directed mutagenesis studies facilitated the identification of a specific Glu that appears central in the transport mechanism. This residue is located in the cytoplasm-membrane interface of transmembrane helix 6 in Na^+-PPases, but shifted to within the membrane or helix 5 in H^+-PPases. These results contribute to the prediction of the transport specificity and K^+ dependence for a particular membrane PPase sequence based on its position in the phylogenetic tree, identity of residues in the K^+ dependence signature and the position of the membrane-located Glu residue.

Membrane pyrophosphatases (PPases; EC 3.6.1.1; Transporter Classification DataBase number 3.A.10) couple the hydrolysis of inorganic pyrophosphate (PP_i) to the active transport of cations across membranes, and display no sequence homology to any known protein family. Membrane PPases consist of 70–81 kDa subunits that apparently form a homodimer (1) and are divided into K^+-dependent and -independent subfamilies. The key determinant of K^+ dependence is a single amino acid position located near the cytoplasm–membrane interface, which is occupied by Ala in the K^+-dependent and Lys in the K^+-independent enzymes (2). All PPases additionally require Mg^{2+} for function (3).

H^+-transporting PPases (H^+-PPases), discovered more than 40 years ago, are widespread among organisms in all three domains of life (4-6). Both K^+-dependent and -independent H^+-PPases have been characterized. In bacteria and archaea, these enzymes generate an ion motive force for ATP synthesis and transport processes, particularly during stress and low energy conditions (7-9). In eukaryotes, H^+-PPase acts in parallel with H^+-ATPase and plays important roles in securing acidity, and thus the functionality of cellular organelles, such as vacuoles in plants (1,6,10) and acidocalcisomes in protozoa (11). In plants, H^+-PPase appears to be involved in auxin-dependent organ development (12-13), and overexpression of the pump in agricultural plants confers resistance against water/nutrient deprivation, cold and salinity (14-17).

Furthermore, H^+-PPase is a promising drug target in protozoan parasites (18).

In contrast, Na^+-transporting PPases (Na^+-PPases) were only recently identified in the mesophilic archaeon *Methanosarcina mazei*, moderately thermophilic acetogenic bacterium *Moorella thermoacetica*, and marine hyperthermophilic bacterium *Thermotoga maritima* (19). These enzymes are similar to the H^+-transporting PPases in many aspects but require both K^+ and Na^+ for activity (20).

The initial discovery of Na^+-PPases in the contrasting ecological and evolutionary niches suggests that PP_i-energized Na^+ transport is a ubiquitous process. However, verification of this hypothesis has been severely hampered by our inability to predict transport specificity directly from protein sequence information. In this study, we overcame this limitation by experimentally screening transport specificity across different types of membrane PPases. These data, in conjugation with phylogenetic analysis, indicate that Na^+ transport specificity is indeed a very common property and precedes H^+ transport specificity in the evolutionary history of the protein family. We additionally employed site-directed mutagenesis to identify the structural elements defining membrane PPase transport specificity.

EXPERIMENTAL PROCEDURES

Sequence and Phylogenetic Analyses—Membrane PPase protein sequences were retrieved from the NCBI protein sequence databank with Blast (21) using *Rhodospirillum rubrum* H^+-PPase (YP_426905) as a query sequence. Protein sequences were aligned using default settings in Muscle version 3.6 (22). The alignment was manually cured by eliminating incomplete and redundant sequences (leaving 121 taxa) and sequence regions, including indels and ambiguously aligned residues (leaving 333 amino acid columns). Input for Bayesian inference of protein phylogeny with MrBayes (23-24) was either the alignment block or partitioned data set where the identity of the experimentally verified K^+ dependence signature sequence was weighted by supplementing the sequence alignment with 398 columns of 0 or 1 characters, depending on whether the full protein sequence harbored Ala (indicative of K^+ dependence) or Lys (K^+ independence), respectively, at position 460 (Ch-PPase numbering). In the weighted tree, topology was estimated utilizing the information content of both partitions, while the amino acid alignment partition defined branch length. Four independent weighted and unconstrained phylogenetic analyses were initiated from random trees and run for 10 million generations (temperature option, 0.15) on a computer cluster provided by the CSC — IT Center for Science, Finland. The average standard deviation of split frequencies between independent MrBayes runs dropped below 0.01 during the first 2.5 million generations, indicating convergence of phylogenetic analysis. The consensus tree was summarized from the last 7.5 million generations. The likelihoods of constrained and unconstrained tree topologies were compared with the Shimodaira–Hasegawa test in Puzzle software using several different settings (25-26). Ancestral protein sequences at internal nodes of the phylogenetic tree were inferred with maximum likelihood method using PAML version 4.4 (27). The likelihood of each possible amino acid state was calculated, given the sequence alignment, topology of the phylogenetic tree, JTT amino acid replacement model, and gamma distribution of among-site rate variations.

Expression of Recombinant Membrane PPases—Genes encoding membrane PPases from *Anaerostipes caccae* (Ac-PPase), *Chlorobium limicola* (Cl-PPase), *Clostridium thermocellum* (Ct-PPase), *Desulfuromonas acetoxidans* (Da-PPase), *Flavobacterium johnsoniae* (Fj-PPase), *Leptospira biflexa* (Lb-PPase), *Pyrobaculum aerophilum* (Pa-PPase), and *Streptomyces coelicolor* (Sc-PPase) were amplified from genomic DNA using the primers listed in Supplementary Table S1. The codon usage-optimized gene for *Clostridium tetani* E88 membrane PPase (Ctet-PPase) was synthesized by Mr. Gene (Regensburg, Germany). Full-length PPase genes were inserted into the multiple cloning site of the pET36b(+) expression vector (Novagen) under T7 promoter control via the *Nde*I, *Xho*I or *Hind*III restriction sites (Supplementary Table S1). The cloning of *T. maritima* Na^+-PPase (Tm-PPase) and *Carboxydothermus hydrogenoformans* H^+-PPase (Ch-PPase) has been described previously (2,20). Amino acid substitutions were engineered with

inverse PCR using Phusion DNA polymerase (Finnzymes), and mutated genes transferred into the pET36b(+) vector. The PPase-encoding regions of the final expression constructs were sequenced.

Membrane PPase genes were expressed in *Escherichia coli*, and inner membrane vesicles (IMV) isolated as described previously (20). IMV were suspended in storage buffer (10 mM Mops-TMA hydroxide, pH 7.2, 1 mM $MgCl_2$, 750–900 mM sucrose, 5 mM DTT, 50 μM EGTA), frozen in liquid N_2, and stored at –85°C. The protein content of IMV was estimated with the Bradford assay (28).

Assay of Hydrolytic Activity—Since *E. coli* lacks endogenous membrane PPase and the IMV isolation protocol efficiently washes away soluble *E. coli* PPase contamination (with <1 % remaining background PPase activity), the IMV prepared from cells carrying membrane PPase expression plasmids could be used directly for activity measurements. To assay membrane PPase hydrolytic activity, a thermostated reaction vessel was filled with 25 mL of reaction buffer typically containing 0.1 M Mops-TMA hydroxide, pH 7.2, 5 mM $MgCl_2$, 158 μM TMA_4PP_i, 40 μM EGTA, and variable concentrations of NaCl and KCl. In measurements of K^+ or Na^+ dependence of PPase activity at a constant concentration (50 mM) of the other ion, TMA hydroxide was replaced with NaOH and KOH, respectively. The reaction was triggered by the addition of IMV suspension (0.004–1.3 mg protein) and liberation of inorganic phosphate continuously recorded for 2–3 min with a flow-through phosphate analyzer (29). Reaction rates were calculated from the initial slopes of the P_i liberation traces. The results of duplicate measurements were usually consistent within 10%.

The dependencies of PP_i hydrolysis rates (v) on Na^+ and K^+ concentrations at saturating substrate and Mg^{2+} concentrations were analyzed in terms of Schemes 1A and 1B, respectively. ES represents the enzyme–substrate complex, M the alkali metal ligand (Na^+ or K^+), K_a and K_i the metal binding constants, and V_1 and V_2 the maximal velocities for the corresponding complexes. Scheme 1A assumes that binding of the first Na^+ ion stimulates hydrolysis, whereas binding of the second Na^+ ion inhibits the reaction. According to Scheme 1B, K^+ binding only modulates hydrolytic activity ($V_1 \neq V_2$). Assuming rapid equilibrium cation binding, rate equations for the mechanisms in Scheme 1A and B are provided by Equations 1 and 2, respectively. Parameter values were determined by fitting these equations to rate data using Scientist software (MicroMath), wherein [M] was treated as an independent variable, v as experimentally measured variable, and V_1, V_2, K_a and K_i as adjustable parameters.

A

$$\begin{array}{ccccc} & & K_a & & K_i & \\ \mathrm{ES} & \leftrightarrow & \mathrm{ESM} & \leftrightarrow & \mathrm{ESM_2} \\ & & \downarrow V_1 & & \end{array}$$

B

$$\begin{array}{ccc} & K_a & \\ \mathrm{ES} & \leftrightarrow & \mathrm{ESM} \\ \downarrow V_2 & & \downarrow V_1 \end{array}$$

SCHEME 1. **Alkali cation (M) binding to the enzyme–substrate complex (ES).** *A*, Na^+ binding; *B*, K^+ binding.

$$v = \frac{V_1}{1 + K_a/[\mathrm{M}] + [\mathrm{M}]/K_i} \qquad \text{(Eq. 1)}$$

$$v = \frac{V_1 + V_2 K_a/[\mathrm{M}]}{1 + K_a/[\mathrm{M}]} \qquad \text{(Eq. 2)}$$

Assay of Transport Activities—PP_i-energized H^+ transport into IMV was assayed by measuring the fluorescence quenching of the pH-sensitive probe, 9-amino-6-chloro-2-methoxyacridine (ACMA, Invitrogen), at 25°C at excitation and emission wavelengths of 428 and 475 nm, respectively. IMV (0.2–1.2 mg) were incubated for 5 min in 2 ml of buffer H (20 mM Mops-TMA hydroxide, pH 7.2, 5 mM $MgCl_2$, 8 μM EGTA, 2 μM ACMA) supplemented with 1.5–25 mM NaCl and 0–100 mM KCl before the reaction was initiated by the addition of 0.3 mM TMA_4-PP_i. The reversibility of ACMA fluorescence quenching was tested by disrupting the H^+ gradient formed in IMV via addition of 10 mM NH_4Cl.

PP_i-energized Na^+-transport into IMV was assayed by determining accumulation of $^{22}Na^+$ within IMV at 22°C. IMV (0.15–0.30 mg) were incubated for ~1 h in 40 μl of buffer N (100 mM

Mops-TMA hydroxide, pH 7.2, 5 mM $MgCl_2$, 50 mM KCl, 1 mM NaCl) containing 0.3–2.5 μCi $^{22}NaCl$ (Perkin Elmer) before the transport reaction was initiated by the addition of 1 mM TMA_4-PP_i. At various time-points, IMV were separated from the reaction medium by passing 30 μl aliquots through a nitrocellulose filter (0.2 μm pore size, 13 mm in diameter, Millipore). External $^{22}Na^+$ was rinsed off by applying 1 ml buffer W (5 mM Mops-TMA hydroxide, pH 7.2, 100 mM NaCl, 0.5 mM $MgCl_2$) through the filter. The filter was transferred to a microcentrifuge tube, 1 mL of Ultima Gold cocktail (PerkinElmer) added, and the amount of $^{22}Na^+$ trapped in IMV determined via liquid scintillation counting.

RESULTS

Updated Phylogenetic Tree and Selection of PPases for Expression—The number of full-length putative membrane PPase sequences in GenBank has increased from about 200 to 1000 since the previous phylogenetic analysis (19). Accordingly, a new tree has been constructed based on 121 nonredundant sequences. The known membrane PPases share 48% average and ≥33% pairwise amino acid identities. Sequence conservation is particularly strong in three cytoplasmically oriented loops forming the major portion of the PP_i hydrolysis site (6). The polypeptides are very hydrophobic, typically containing 16 predicted transmembrane α-helices. In a few cases, more transmembrane α-helices have been identified in N- or C-terminal extensions to the core structure.

MrBayes analysis generated a tree largely consistent with the previously determined grouping of PPases into K^+-dependent and -independent subfamilies (2). Notably, sequences from *C. thermocellum* and *Thermotoga lettingae* were grouped with K^+-dependent enzymes near the boundary between the subfamilies, although they possessed sequence determinants (K478 and T481, Cl-PPase numbering) of K^+ independence (Figure 1). To assess the significance of anomalous grouping, we shifted the *C. thermocellum* and *T. lettingae* sequences to the K^+-independent subfamily by heavily weighting the experimentally determined K^+ dependence signature and comparing the resulting tree with an unconstrained tree using the Shimodaira–Hasegawa test implemented in Puzzle software (25). The constrained tree appeared to have a higher likelihood, while the unconstrained tree was significantly rejected ($p<0.05$). Accordingly, the constrained tree was utilized for all further analyses.

To comprehensively map the distribution of transport specificities among membrane PPases, we selected several key genes from the constructed phylogenetic tree for the expression and biochemical characterization of the corresponding expressed proteins. We focused on PPases located in hitherto unexplored clades within the phylogenetic tree. In total, seven PPase sequences were selected for analysis.

Expression of Functional PPases in E. coli—Novel membrane PPases were heterologically expressed in *E. coli* and the recombinant proteins isolated as *E. coli* IMV. We additionally expressed four previously described membrane PPases (from *C. hydrogenoformans*, *P. aerophilum*, *S. coelicolor*, and *T. maritima*). All PPases were expressed in the active form, as determined using two criteria. Firstly, Western analysis of IMV proteins using rabbit antiserum raised against a conserved amino acid motif in the third cytoplasmic loop of the enzyme (19) revealed specific bands representing proteins of predicted sizes (Supplementary Figure S1). Second, the IMV exhibited increased PP_i hydrolytic activity, which was suppressed by the membrane PPase inhibitor, aminomethylenediphosphonate (AMDP), but insensitive to the *E. coli* soluble PPase inhibitor, fluoride (30) (Figure 2).

Maximal PP_i hydrolysis activities of Ch-PPase, Ct-PPase, Pa-PPase, and Tm-PPase were relatively low at 25°C (5–50 $nmol \cdot min^{-1} \cdot mg^{-1}$) but increased at least 3-fold when the assay temperature was increased to 40°C (Figure 2), consistent with the fact that the genes encoding these membrane PPases were isolated from thermophilic host organisms. Importantly, Ct-PPase activity at 40°C (and 25°C) was independent of the K^+ concentration (Figure 2), leading to its classification as a member of the K^+-independent subfamily. This finding further supports the validity of the constrained phylogenetic tree.

Ion Transport Activities of PPases—The H^+ transport capacity of all PPases was assayed by monitoring fluorescence of a pH indicator, 9-

amino-6-chloro-2-methoxyacridine (ACMA), at 25ºC. When PP_i was added to the reaction mixture containing Lb-PPase-, Fj-PPase, and Ch-PPase-harboring IMV, dye fluorescence progressively decreased to a steady-state level indicating acidification of the IMV lumen (Figure 3, panel A). Upon disruption of the proton gradient with the addition of NH_4Cl or consumption of all PP_i, fluorescence returned to the initial level. Qualitatively similar fluorescence changes were previously observed for Ch-PPase IMV by employing acridine orange as the pH indicator (2). Given the lack of PP_i-dependent IMV acidification in native *E. coli* vesicles devoid of membrane PPases, it is proposed that the observed H^+ transport activity is specifically mediated by recombinant PPases.

In contrast, no H^+ transport activity was detected with Ac-PPase, Cl-PPase, Ct-PPase, Ctet-PPase and Da-PPase. To ascertain whether this finding was due to low PPase activity at 25ºC, we estimated the sensitivity of the transport assay. To this end, we recorded the H^+ transport signal mediated by Lb-PPase under conditions where it was tuned to low activity by decreasing K^+- and Na^+-concentrations (Figure 3, panel B). In this setup, Lb-PPase IMV produced the lowest detectable H^+ transport signal in the presence of 1.5 mM Na^+ corresponding to a PP_i hydrolysis rate of 13 $nmol \cdot min^{-1} \cdot mg^{-1}$. The hydrolytic activities of most PPases under conditions of H^+ transport measurements were well above this limit, and the lack of the H^+ transport signal for a particular PPase was strongly indicative of its inability to perform this function. The only exception was Ct-PPase, whose activity (5 $nmol \cdot min^{-1} \cdot mg^{-1}$) was too low to support measurable H^+ transport activity. Unfortunately, high temperatures are unattainable for H^+ transport experiments with *E. coli* IMV, since the passive permeation rate across the membrane rises steeply with temperature.

Na^+ transport activity was determined with a filtration assay utilizing ^{22}Na. The active transport reaction was initiated by adding PP_i to IMV preequilibrated with $^{22}Na^+$. Significant transport rates were observed with Ac-PPase, Cl-PPase, Ctet-PPase, Da-PPase and Tm-PPase (Figure 4). These findings led to the identification of four new Na^+-transporting PPases (marked with asterisks in Figure 4 and all subsequent figures and tables) and confirmed our earlier characterization of Tm-PPase as a Na^+ pump using a different transport assay (19). No Na^+ transport was observed with the other membrane PPases examined in this study (Figure 4).

Previous studies have reported that membrane PPases from *S. coelicolor* (Sc-PPase), *M. mazei* (Mm-PPase 2), *R. rubrum* (R-PPase) and *A. thaliana* (AVP 2) belonging to the K^+-independent subfamily and the K^+-dependent enzyme from *C. hydrogenoformans* mediate PP_i-dependent H^+ transport activity (2,31-34), while R-PPase has no Na^+ transport activity (19). Our current results consistently demonstrate that Pa-PPase, Sc-PPase and Ch-PPase do not mediate Na^+-transport into IMV (Figure 4). The activities of K^+-independent H^+-PPases and Ch-PPase appear thus to be specifically related to H^+ transport.

Notably, the Na^+ transport assay was more sensitive than the H^+ transport assay. Despite the relatively low PP_i hydrolytic activity of hyperthermophilic Tm-PPase (14 $nmol \cdot min^{-1} \cdot mg^{-1}$) at the assay temperature (22ºC), the enzyme catalyzed significant time-dependent $^{22}Na^+$ accumulation into IMV (Figure 4, see also inset). Moreover, the $^{22}Na^+$ transport signal was at least three-fold higher than the background, even under conditions (1.5 mM K^+ and 1 mM Na^+) where Tm-PPase hydrolytic activity was as low as 5 $nmol \cdot min^{-1} \cdot mg^{-1}$ (data not shown). Since the hydrolytic activities of all PPases producing no Na^+ transport signal were equal to or exceeded this value (Figure 2), we concluded that these enzymes possess no Na^+ transport activity. This result is consistent with the above finding that PPases (except Ct-PPase) are active as H^+ transporters. Ct-PPase did not exhibit any transport activity, but given the lower sensitivity of the H^+ transport assay, it is likely that Ct-PPase operates as a H^+ transporter in *C. thermocellum* at its growth temperature (60ºC). This may also apply to the *P. aerophilum* enzyme (Pa-PPase), another thermophilic enzyme for which no H^+ transport signal was observed in earlier studies (35).

Na^+ and K^+ Dependencies of PPase Activity—H^+-transporting PPases are either active in the absence of alkali cations or require K^+ for activity (6), whereas Na^+-transporting PPases absolutely require Na^+ and are further activated by K^+ (19). To determine the alkali cation requirements of the newly expressed membrane PPases, we measured their hydrolytic activities

over a wide range of Na^+ and K^+ concentrations. No activity exceeding the background *E. coli* soluble PPase-attributable value was observed in the absence of both Na^+ and K^+.

The Na^+ dose-response curves measured in the absence of K^+ were similar for all PPases, except that low-level inhibition of Cl-PPase was observed at high [Na^+] (Figure 5). These curves appear to reflect the findings that Na^+-transporting PPases absolutely require Na^+ for activity and that Na^+ can partially meet the K^+ requirement of K^+-dependent H^+-transporting PPases (3,20).

Significant alterations in the dose-response curves were observed when PP_i hydrolysis was assayed in the presence of 50 mM K^+. First, the maximal activity values increased in all cases. Second, the curves for the Na^+-transporting PPases shifted to lower Na^+ concentrations. Third, the H^+-transporting PPases lost their response to Na^+ concentrations (Lb-PPase) or Na^+ became inhibitory (Fj-PPase). The latter observation is consistent with a lower capacity of Na^+ to activate K^+-dependent H^+-transporting PPases, compared with K^+ (3). Additionally, inhibition by excess Na^+ was more pronounced with Cl-PPase. The parameter values for Scheme 1A (one activating and one inhibiting Na^+) obtained using Equation 1 are summarized in Table 1. In terms of maximal activity (V_1) and activating Na^+ binding constant (K_a), K^+ enhanced the maximal rate of PP_i hydrolysis 2 to 11-fold and Na^+ binding affinity 40–400-fold in different Na^+-PPases (Table 1). The novel Na^+-PPases thus appear to utilize the same bi-functional mechanism of K^+ activation as those described previously (19-20), i.e., K^+ increases both the Na^+ binding affinity and catalytic constant. In contrast to Na^+-PPases, which require both Na^+ and K^+ for maximal activity, K^+ alone is sufficient for full activation of H^+-transporting Fj- and Lb-PPases (Figure 5). Accordingly, these PPases have been classified as K^+-dependent enzymes.

It is possible that in Fj-PPase and Cl-PPase, the Na^+-binding constants (K_a) measured in the absence of K^+ and K_i measured in the presence of K^+ refer to the same binding site, and the difference between these constants reflects competition with K^+ in the latter case. The K^+ binding constant for Fj-PPase can be thus estimated from the data as 3.7 mM, compared with 9 mM for Na^+.

At a fixed concentration of 50 mM Na^+ and increasing K^+ concentrations, the hydrolytic activities of all PPases increased from a non-zero basal to maximal level (Figure 6). The activation profile is modeled in Scheme 1B assuming a single activating K^+ binding site on the enzyme. The K^+-binding constant, K_a, was in the range of 14–38 mM (Table 2), and did not change systematically between Na^+- and H^+-transporting PPases.

The Role of Membrane-Located Glu in Ion Transport Specificity—Extensive manual or computational (Sequence Harmony) (36) search for sequence determinants correlating with enzyme transport specificities failed to identify a single pattern of residue conservation matching the observed transport specificities across the entire phylogenetic tree. The evolutionary history of membrane PPases therefore appears to include more than one change in transport specificity. Comparison of Na^+-PPases and plant-type H^+-PPases revealed a single conserved Glu residue (Glu^{242} in Cl-PPase) in all characterized Na^+-PPases near the cytoplasmic end of transmembrane helix 6 (TMH 6), which serves as a membrane anchor for the highly conserved and functionally important cytoplasmic loop (31) (residue 242 in Figure 1). In plant-type H^+-PPases (including bacterial Lb-PPase), Glu is shifted by four residues towards the C-terminal end of the polypeptide and becomes membrane-buried. Interestingly, TMH 6 is completely devoid of the relevant Glu in Fj-PPase-type H^+-pumps (sequences from *F. johnsoniae* to *A. asiaticus* in Figure 1). In these enzymes, a conserved Glu is found instead in the preceding TMH 5 in the position aligned with Cl-PPase residue 180. As conserved charged residues are not present in TMH 5 in other types of membrane PPases, it is proposed that the Glu residue is specifically relocated from TMH 6 to TMH 5.

Since two independent Glu relocations are correlated with changes in ion transport specificity, we employed site-directed mutagenesis to study the functional consequences of engineered Glu substitutions and relocation.

Initially, we relocated the Glu residues in TMH 5 of Fj-PPase and TMH 6 of Lb-PPase to the conventional Na^+-PPase position at the cytoplasm-membrane interface in TMH 6. We additionally replaced Gly 246 of *C. limicola* Na^+-PPase with

Ala, like in *F. johnsoniae* H^+-PPase, and transferred the Glu from TMH 6 to TMH 5 independently or in combination with the Gly→Ala substitution. The resulting recombinant variants (Fj-PPase E185S/G247E, Lb-PPase G249E/E253G, Cl-PPase S180E/E242G, Cl-PPase S180E/E242G/G246A, and Cl-PPase G246A) retained expression in *E. coli* (Supplementary Figure S1), but were inactive. Thus, membrane PPase poorly tolerates substitutions that increase amino acid sizes, possibly due to tight packing of the transmembrane helices.

To avoid potential steric clashes, we replaced Glu with Asp in the second round of mutagenesis. The variant enzymes, Fj-PPase E185D, Lb-PPase E253D, and Cl-PPase E242D, retained 24%, 32%, and 37% of wild-type PP_i hydrolysis activity, respectively. The transport data recorded for the variant enzymes indicated decreased transport rates in keeping with decreased enzymatic activity, but no changes in transport specificity (Figures 3 and 4). Most importantly, the Na^+ dose-response curve of the Cl-PPase E242D variant was dramatically shifted to higher Na^+ concentrations, relative to the wild-type enzyme (Figure 5). Accordingly, the Na^+ binding constant (K_a) for the activating Na^+ ion increased up to 450-fold (Table 1). In contrast, K^+ binding affinity was not significantly affected (Figure 6 and Table 2).

In the third round of mutagenesis, the carboxyl group of the Glu residue under consideration was eliminated by substitution to Ser. The E242S substitution appeared to structurally destabilize Cl-PPase, since no variant polypeptides were detected in the IMV fraction using Western analysis. Fj-PPase E185S and Lb-PPase E253S variants retained 20–30% of wild-type PPase activity, respectively, but exhibited no detectable PP_i-dependent H^+ or Na^+ transport activity (Figures 3 and 4). Hydrolytic activities of both variant PPases were sufficiently high (>85 $nmol \cdot min^{-1} \cdot mg^{-1}$) to generate a recordable H^+ or Na^+ transport signal (see above). Furthermore, IMV leakage was not significantly affected by membrane PPase substitutions, since in all tested cases, the IMVs supported comparable levels of ATP-dependent H^+-gradient generated by *E. coli* housekeeping enzymes. These results suggest that Glu^{242} (Cl-PPase numbering) is a critical but not the sole determinant of transport specificity in membrane PPases.

DISCUSSION

The membrane PPase family consists of two independently evolving subfamilies, one (K^+-dependent) requiring millimolar concentrations of K^+ to attain catalytic activity and the other being K^+-independent (2). Both subfamilies were originally believed to operate as H^+ pumps until the recent discovery of Na^+-transporting PPases within the K^+-dependent subfamily (19). The four novel Na^+-transporting PPases uncovered in this study have further increased the total number of identified Na^+-PPases to seven. Moreover, Biegel and Müller (37) recently reported PP_i-dependent Na^+ accumulation in IMV prepared from *Acetobacterium woodii*, suggesting that this bacterium also contains a Na^+-transporting PPase. Notably, Ctet-PPase was previously reported to operate as a H^+ pump (38). We did not observe a PP_i-induced H^+ transport signal with Ctet-PPase IMV, but detected a strong Na^+ transport signal. Ctet-PPase has thus been classified as a Na^+ pump, consistent with the findings that *C. tetani* employs Na^+ as the major coupling ion for membrane transport processes, lacks primary H^+-pumps, and has a V-type Na^+-coupled ATPase instead of H^+-ATPase (39).

K^+-dependent PPases can be phylogenetically classified into four major clades rooting at nodes A, B, C and D (Figure 1). Clade A branches at the interface of K^+-dependent and independent subfamilies, whereas clades B, C and D group monophyletically at node N further within the K^+-dependent subfamily. Clade A contains H^+-PPases, clades B and C are populated by Na^+-PPases whereas clade D possesses both H^+- and Na^+-PPases. Na^+-PPases thus dominate the K^+ dependent subfamily, whereas Na^+ pumping/dependence are traced to node N and thus considered an ancestor of the N cluster (groups of B, C, and D clades). At the functional level, the monophyletic origin of all existing Na^+-PPases is supported by the finding that the activities of the enzymes characterized are regulated similarly by a complex Na^+- and K^+-dependent mechanism affecting both maximal enzymatic activity and ligand binding affinities. Two scenarios are envisaged to explain the presence of H^+-PPases in clade D, specifically, placing of H^+-PPase in clade D is an artifact of

phylogenetic reconstitution or the H^+ specificity of some PPases in clade D is not homologous to that of clade A and K^+-independent H^+-PPases, but a result of homoplasy. Our analysis of the Glu residues in TMH 5 and 6 favors the latter possibility.

The three subtypes of clade D membrane PPases are represented by Na^+-transporting Cl-PPase, H^+-transporting Fj-PPase, and plant-type H^+-PPases. Cl-PPase is similar to enzymes from evolutionarily diverse bacteria. Fj-PPase has close homologs only among Bacteroidetes whereas the plant category of H^+-PPases additionally includes enzymes from unicellular protozoa and spirochaete bacteria Leptospira. H^+-transporting Fj-PPase and plant enzymes group polyphyletically and differ from all Na^+-PPases and the clade D ancestor enzyme in that Glu^{242} (Cl-PPase numbering) is relocated from its cytoplasm-membrane interface position in TMH 6 to a membrane-embedded position in TMH 5 or TMH 6, respectively. Several lines of evidence support the hypothesis that Glu^{242} relocations are key, albeit not the only structural modifications during the evolutionary pathways responsible for the H^+ transport specificity of Fj-PPase type and Leptospira/protozoa/plant-type enzymes. First, site-directed mutagenesis data indicate an essential role for TMH 5 and TMH 6 carboxyl groups in maintaining PP_i hydrolysis coupling to H^+ transport across the membrane. This conclusion is further supported by the recently published results of alanine scanning mutagenesis study of TM6 of mung bean H^+-PPase (40). Second, N,N′-dicyclohexylcarbodiimide that preferentially reacts with protonated carboxyl groups targets the relevant Glu in *A. thaliana* H^+-PPase (AVP1) (41). Finally, the $Glu^{242}\rightarrow$Asp substitution leads to a dramatic increase in the Na^+ concentration required for maximal activity of Na^+-PPase in the presence of K^+, indicating changes in the affinity of the Na^+-specific binding site that presumably functions as the cytoplasmic acceptor for the transported Na^+ (42).

K^+-independent enzymes from *C. thermocellum* and *T. lettingae* are phylogenetically the most closely related to K^+-dependent PPases. Ct-PPase and Pa-PPase do not transport Na^+ and may thus perform H^+ transport activity similar to other characterized K^+-independent membrane PPases, but this is yet to be directly demonstrated. Since five characterized K^+-independent H^+-PPases represent distinct divergent clades within the subfamily and no K^+-independent Na^+-PPases have been encountered so far, it is highly likely that all members of the K^+-independent subfamily operate as H^+ pumps.

Significantly, the Na^+-PPase and K^+-independent H^+-PPase genes are adjacent in the *M. mazei* genome, suggesting that the gene cluster is a footprint of an ancient gene duplication event resulting in the formation of the two deeply rooted subfamilies. To date, the classification of membrane PPases has been based on their requirement for K^+. However, we speculate that initial specialization of the duplicates leading to emergence of two subfamilies was, in fact, driven by changes in transported cation specificity and followed by secondary loss of K^+ dependence in H^+-PPases. Indeed, the absence of K^+-independent Na^+-PPases and our failure to generate such enzymes via mutagenesis (G.B. and H.L., unpublished) suggests that K^+ independence is incompatible with Na^+ pumping. The change in transport specificity adds to the capability of the organism to utilize PP_i for the generation of both Na^+ and H^+ gradients, while changes in K^+ dependency do not provide an immediate fitness benefit. We further propose that the ancestor enzyme is possibly a Na^+ pump. Thus, the evolution of a membrane PPase coupling ion specificity from Na^+ to H^+ parallels the scenario suggested for Na^+- and H^+-coupled F- and V-type ATP synthases/ATPases and adds support to the concept of global evolutionary primacy of Na^+-coupled bioenergetics (43-45,53).

Further research is required to establish the physiological role of Na^+-transporting PPase. A literature search has revealed two interesting trends. First, Na^+-PPase is more frequently found in anaerobic organisms than H^+-PPase. Thus, 23 of the 30 characterized and predicted Na^+-PPases in the phylogenetic tree (Figure 1) are derived from anaerobic hosts, whereas only 14 of 49 H^+-PPases belong to anaerobes. Thus, a change from an anaerobic to aerobic environment may have provided the driving force for evolution from PP_i-energized Na^+ pumping to H^+ pumping. This is most evident in clade D, which contains 4 of 7 aerobic Na^+-PPases (compared to only 3 of 25 Na^+-PPases from aerobic hosts in clades B and C). Secondly, at least half the anaerobic and all except

one aerobic Na^+-PPase hosts are halophilic or halotolerant, compared to only a quarter of H^+-PPases. Accordingly, it is proposed that Na^+-PPase function is related to creating salt tolerance, especially in aerobic host organisms. This theory may be extended to speculate that since Na^+-PPase is naturally preferred in halophiles, this enzyme may prove better than H^+-PPase (6) in engineering salt tolerance in plants/microbes.

In summary, our results confirm that a wide range of microorganisms employ PP_i-energized Na^+ extrusion systems. We provide a comprehensive reconstruction of membrane PPase evolution and predict the transport specificity of membrane PPases as follows: (i) K^+-independent enzymes are proton pumps, (ii) K^+-dependent enzymes belonging to clade N are sodium pumps if Glu is present at the TMH6 interface and proton pumps if the Glu residue is relocated, and (iii) K^+-dependent enzymes belonging to clade A are proton pumps. Notably, the sequence determinants governing the differences in transport specificity between clades A and N are not fully clarified at present, and therefore, the position of the sequence in the phylogenetic tree is an essential part of the prediction algorithm.

REFERENCES

1. Maeshima, M. (2000) *Biochim. Biophys. Acta.* **1465**, 37–51
2. Belogurov, G. A., and Lahti, R. (2002) *J. Biol. Chem.* **277**, 49651–49654
3. Baykov, A. A., Bakuleva, N. P., and Rea, P. A. (1993) *Eur. J. Biochem.* **217**, 755–762
4. Baltscheffsky, M. (1967) *Nature* **216**, 241–243
5. Baltscheffsky, H., Von Stedingk, L. V., Heldt, H. W., and Klingenberg, M. (1966) *Science* **153**, 1120–1122
6. Serrano, A., Perez-Castineira, J. R., Baltscheffsky, M., and Baltscheffsky, H. (2007) *IUBMB Life* **59**, 76–83
7. Baltscheffsky, M., Schultz, A., and Baltscheffsky, H. (1999) *FEBS Lett.* **457**, 527–533
8. Lopez-Marques, R. L., Perez-Castineira, J. R., Losada, M., and Serrano, A. (2004) *J. Bacteriol.* **186**, 5418–5426
9. Garcia-Contreras, R., Celis, H., and Romero, I. (2004) *J. Bacteriol.* **186**, 6651–6655
10. Drozdowicz, Y. M., and Rea, P. A. (2001) *Trends Plant Sci.* **6**, 206–211
11. Docampo, R., de Souza, W., Miranda, K., Rohloff, P., and Moreno, S. N. (2005) *Nat. Rev. Microbiol.* **3**, 251–261
12. Fukuda, A., and Tanaka, Y. (2006) *Plant Physiol. Biochem.* **44**, 351–358
13. Li, J., Yang, H., Peer, W. A., Richter, G., Blakeslee, J., Bandyopadhyay, A., Titapiwantakun, B., Undurraga, S., Khodakovskaya, M., Richards, E. L., Krizek, B., Murphy, A. S., Gilroy, S., and Gaxiola, R. (2005) *Science* **310**, 121–125
14. Zhang, J., Li, J., Wang, X., and Chen, J. (2011) *Plant Physiol. Biochem.* **49**, 33–38
15. Lv, S., Zhang, K., Gao, Q., Lian, L., Song, Y., and Zhang, J. (2008) *Plant Cell Physiol.* **49**, 1150–1164
16. Li, B., Wei, A., Song, C., Li, N., and Zhang, J. (2008) *Plant Biotechnol. J.* **6**, 146–159
17. Park, S., Li, J., Pittman, J. K., Berkowitz, G. A., Yang, H., Undurraga, S., Morris, J., Hirschi, K. D., and Gaxiola, R. A. (2005) *Proc. Natl. Acad. Sci. U S A* **102**, 18830–18835
18. Docampo, R., and Moreno, S. N. (2008) *Curr. Pharm. Des.* **14**, 882–888
19. Malinen, A. M., Belogurov, G. A., Baykov, A. A., and Lahti, R. (2007) *Biochemistry* **46**, 8872–8878
20. Belogurov, G. A., Malinen, A. M., Turkina, M. V., Jalonen, U., Rytkonen, K., Baykov, A. A., and Lahti, R. (2005) *Biochemistry* **44**, 2088–2096
21. Altschul, S. F., Gish, W., Miller, W., Myers, E. W., and Lipman, D. J. (1990) *J. Mol. Biol.* **215**, 403–410
22. Edgar, R. C. (2004) *Nucleic Acids Res.* **32**, 1792–1797
23. Ronquist, F., and Huelsenbeck, J. P. (2003) *Bioinformatics* **19**, 1572–1574
24. Huelsenbeck, J. P., and Ronquist, F. (2001) *Bioinformatics* **17**, 754–755

25. Shimodaira, H., and Hasegawa, M. (1999) *Mol. Biol. Evol.* **16**, 1114–1116
26. Schmidt, H. A., Strimmer, K., Vingron, M., and von Haeseler, A. (2002) *Bioinformatics* **18**, 502–504
27. Yang, Z. (2007) *Mol. Biol. Evol.* **24**, 1586–1591
28. Bradford, M. M. (1976) *Anal. Biochem.* **72**, 248–254
29. Baykov, A. A., and Avaeva, S. M. (1981) *Anal. Biochem.* **116**, 1–4
30. Baykov, A. A., Dubnova, E. B., Bakuleva, N. P., Evtushenko, O. A., Zhen, R. G., and Rea, P. A. (1993) *FEBS Lett.* **327**, 199–202
31. Mimura, H., Nakanishi, Y., Hirono, M., and Maeshima, M. (2004) *J. Biol. Chem.* **279**, 35106–35112
32. Baumer, S., Lentes, S., Gottschalk, G., and Deppenmeier, U. (2002) *Archaea* **1**, 1–7
33. Moyle, J., Mitchell, R., and Mitchell, P. (1972) *FEBS Lett.* **23**, 233–236
34. Drozdowicz, Y. M., Kissinger, J. C., and Rea, P. A. (2000) *Plant Physiol.* **123**, 353–362
35. Drozdowicz, Y. M., Lu, Y. P., Patel, V., Fitz-Gibbon, S., Miller, J. H., and Rea, P. A. (1999) *FEBS Lett.* **460**, 505–512
36. Pirovano, W., Feenstra, K. A., and Heringa, J. (2006) *Nucleic Acids Res.* **34**, 6540–6548
37. Biegel, E., and Muller, V. (2011) *J. Biol. Chem.* **286**, 6080–6084
38. Huang, Y. T., Liu, T. H., Chen, Y. W., Lee, C. H., Chen, H. H., Huang, T. W., Hsu, S. H., Lin, S. M., Pan, Y. J., Hsu, I. C., Tseng, F. G., Fu, C. C., and Pan, R. L. (2010) *J. Biol. Chem.* **285**, 23655–23664
39. Bruggemann, H., Baumer, S., Fricke, W. F., Wiezer, A., Liesegang, H., Decker, I., Herzberg, C., Martinez-Arias, R., Merkl, R., Henne, A., and Gottschalk, G. (2003) *Proc. Natl. Acad. Sci. U S A* **100**, 1316–1321
40. Pan, Y. J., Lee, C. H., Hsu, S. H., Huang, Y. T., Liu, T. H., Chen, Y. W., Lin, S. M., and Pan, R. L. (2011) *Biochim. Biophys. Acta* **1807**, 59–67
41. Zhen, R. G., Kim, E. J., and Rea, P. A. (1997) *J. Biol. Chem.* **272**, 22340–22348
42. Malinen, A. M., Baykov, A. A., and Lahti, R. (2008) *Biochemistry* **47**, 13447–13454
43. Mulkidjanian, A. Y., Galperin, M. Y., Makarova, K. S., Wolf, Y. I., and Koonin, E. V. (2008) *Biol. Direct* **3**, 13
44. Mulkidjanian, A. Y., Dibrov, P., and Galperin, M. Y. (2008) *Biochim. Biophys. Acta* **1777**, 985–992
45. Mulkidjanian, A. Y., Galperin, M. Y., and Koonin, E. V. (2009) *Trends Biochem. Sci.* **34**, 206–215
46. Belogurov, G. A., Turkina, M. V., Penttinen, A., Huopalahti, S., Baykov, A. A., and Lahti, R. (2002) *J. Biol. Chem.* **277**, 22209–22214
47. Drozdowicz, Y. M., Shaw, M., Nishi, M., Striepen, B., Liwinski, H. A., Roos, D. S., and Rea, P. A. (2003) *J. Biol. Chem.* **278**, 1075–1085
48. Luo, S., Marchesini, N., Moreno, S. N., and Docampo, R. (1999) *FEBS Lett.* **460**, 217–220
49. Hill, J. E., Scott, D. A., Luo, S., and Docampo, R. (2000) *Biochem. J.* **351**, 281–288
50. Ruiz, F. A., Marchesini, N., Seufferheld, M., Govindjee, and Docampo, R. (2001) *J. Biol. Chem.* **276**, 46196–46203
51. Britten, C. J., Zhen, R. G., Kim, E. J., and Rea, P. A. (1992) *J. Biol. Chem.* **267**, 21850–21855
52. Sarafian, V., Kim, Y., Poole, R. J., and Rea, P. A. (1992) *Proc. Natl. Acad. Sci. U S A* **89**, 1775–1779
53. Holm N.G., and Baltscheffsky H. (April 2, 2011) *Orig. Life Evol. Biosph.* 10.1007/s11084-011-9235-4

FOOTNOTES

*We are sincerely grateful to Dr. Maria Muntyan for helpful advice on the Na^+ transport assay and Dr. Mathieu Picardeau for providing genomic DNA of *L. biflexa*. The research was supported by Academy of Finland Grant 114706, 130581, and 139031, a grant from the Ministry of Education of Finland (for the National Graduate School in Informational and Structural Biology), and the Russian Foundation for Basic Research Grant 09-04-00869.

Abbreviations: Ac-PPase, *Anaerostipes caccae* PPase; ACMA, 9-amino-6-chloro-2-methoxyacridine; AMDP, aminomethylenediphosphonate; AVP1, *Arabidopsis thaliana* PPase 1; Ch-PPase, *Carboxydothermus hydrogenoformans* PPase; Cl-PPase, *Chlorobium limicola* PPase; Ct-PPase, *Clostridium thermocellum* PPase; Ctet-PPase *Clostridium tetani* PPase; Da-PPase, *Desulfuromonas acetoxidans* PPase; DCCD, N,N′-dicyclohexylcarbodiimide; EGTA ethylene glycol bis(2-aminoethyl ether); Fj-PPase, *Flavobacterium johnsoniae* PPase; IMV, inner membrane vesicles; Lb-PPase, *Leptospira biflexa* PPase; MOPS, 4-morpholinepropanesulfonic acid; Mt-PPase, *Moorella thermoacetica* PPase; Pa-PPase, *Pyrobaculum aerophilum* PPase; P_i, inorganic phosphate; PPase, inorganic pyrophosphatase; PP_i, inorganic pyrophosphate; Sc-PPase, *Streptomyces coelicolor* PPase; SDS-PAGE, sodium dodecyl sulfate-polyacrylamide gel electrophoresis; Tm-PPase, *Thermotoga maritima* PPase; TMA, tetramethylammonium; TMH, transmembrane helix

FIGURE LEGENDS

Fig. 1. Phylogenetic tree, residue conservation and functional classification of membrane PPases. The tree was arbitrarily rooted with the branch leading to the *S. coelicolor* clade of H^+-PPase. The GenBank™ protein sequence number is indicated in front of the species name. The nodes are supplemented with clade credibility values and marked in selected cases with capital letters. The studied membrane PPases are placed inside boxes. The scale bar represents 0.2 substitutions per residue. For clarity, only 79 of 121 sequences used to construct the tree are shown. The residue columns 180, 242, 246 (Cl-PPase numbering) to the right of the tree correspond to the positions of the pump specificity-linked Glu residue, while residue columns 478 and 481 refer to the positions determining K^+ requirements. *K^+ dependence* and *Coupling ion* columns present the inferred and experimentally verified K^+ requirement and coupling ion specificity, respectively.

Fig. 2. Hydrolytic activities of recombinant membrane PPases in *E. coli* IMV. Hydrolytic activity was determined at 25°C (*main figure*) or 40°C (*insets*). Unless otherwise indicated, the reaction medium contained 50 mM KCl and 10 mM NaCl (white bars). Grey and black bars depict PPase activity in the presence of 250 μM potassium fluoride and 20 μM AMDP, respectively. The K^+ dose response of Ct-PPase activity was assayed in the absence of added Na^+.

Fig. 3. H^+ transport by membrane PPases at 25°C. The transport reaction was commenced by adding TMA_4-PP_i to the otherwise complete reaction mixture. The fluorescence intensity at 475 nm returned to the initial level when the steady-state proton gradient was collapsed by adding 10 mM ammonium chloride. The incidence of PP_i and ammonium chloride additions is indicated with arrows. (A) Wild-type PPases (measured at 10 mM Na^+ and 50 mM K^+). (B) H^+ transport by Lb-PPase as a function of Na^+ concentration. The respective Lb-PPase hydrolytic activities were 320 (10 mM Na^+ and 50 mM K^+), 75 (25 mM Na^+), 38 (10 mM Na^+), 25 (5 mM Na^+), and 13 (1.5 mM Na^+) $nmol \cdot min^{-1} \cdot mg^{-1}$. (C) Mutant PPases (10 mM Na^+ and 100 mM K^+).

Fig. 4. Na^+ transport by membrane PPases at 22°C. The membrane PPase-catalyzed transport reaction was commenced by adding TMA_4-PP_i to otherwise complete the reaction mixture and allowed to proceed for 1 min. The inset shows the time dependence of Na^+-transport into PPase-free IMV and IMV

containing Tm-PPase or Lb-PPase. The error bars display S.D. for at least three independent measurements. The enzymes classified as Na^+-PPases are indicated with asterisks.

Fig. 5. Dependence of the hydrolytic activities of membrane PPases on Na^+ concentration at 25°C. The K^+ concentration was either zero (upper panel) or 50 mM (lower panel). Lines were obtained with Equation 1 using the best-fit parameter values found in Table 1.

Fig. 6. Dependence of the hydrolytic activities of membrane PPases on K^+ concentrations at 25°C. The Na^+ concentration was 50 mM. Lines were obtained with Equation 2 using the best-fit parameter values found in Table 2.

TABLE 1
Kinetic parameters for Na^+ activation in the presence and absence of 50 mM K^+

Enzyme	Parameter value				
	no K^{+a}		50 mM K^+		
	V_1	K_a	V_1	K_a	K_i
	µmol·min^{-1}·mg^{-1}	*mM*	*µmol·min^{-1}·mg^{-1}*	*mM*	*mM*
Ac-PPase*	0.04 ± 0.01	23 ± 5	0.17 ± 0.01	0.43 ± 0.04	n.a.[b]
Ctet-PPase*	0.24 ± 0.01	27 ± 2	0.80 ± 0.08	0.45 ± 0.08	n.a.
Da-PPase*	0.48 ± 0.08	80 ± 2	0.78 ± 0.09	1.9 ± 0.4	n.a.
Cl-PPase*	0.26 ± 0.04	14 ± 3	1.1 ± 0.1	0.036 ± 0.002	100 ± 20
Cl-PPase (E242D)*	0.38 ± 0.08	190 ± 50	0.81 ± 0.06	16 ± 2	400 ± 110
Fj-PPase	0.09 ± 0.01	9 ± 2	0.99 ± 0.04	n.a.	130 ± 20
Lb-PPase	0.14 ± 0.02	9 ± 2	0.46 ± 0.05	n.a.	n.a.

[a] K_i value was above 1000 mM in the absence of K^+.
[b] n.a = not attendant

TABLE 2
Kinetic parameters for K^+ activation in the presence of 50 mM Na^+

Enzyme	Parameter value		
	V_1	V_2	K_a
	$\mu mol \cdot min^{-1} \cdot mg^{-1}$	$\mu mol \cdot min^{-1} \cdot mg^{-1}$	*mM*
Ac-PPase*	0.25 ± 0.01	0.03 ± 0.01	14 ± 2
Ctet-PPase*	1.9 ± 0.2	0.44 ± 0.04	30 ± 9
Da-PPase*	1.31 ± 0.04	0.15 ± 0.01	38 ± 2
Cl-PPase*	1.2 ± 0.1	0.25 ± 0.02	32 ± 8
Cl-PPase (E242D)*	0.89 ± 0.03	0.06 ± 0.01	19 ± 2
Fj-PPase	1.45 ± 0.08	0.11 ± 0.01	20 ± 2
Lb-PPase	0.74 ± 0.06	0.14 ± 0.01	18 ± 5

Fig. 1

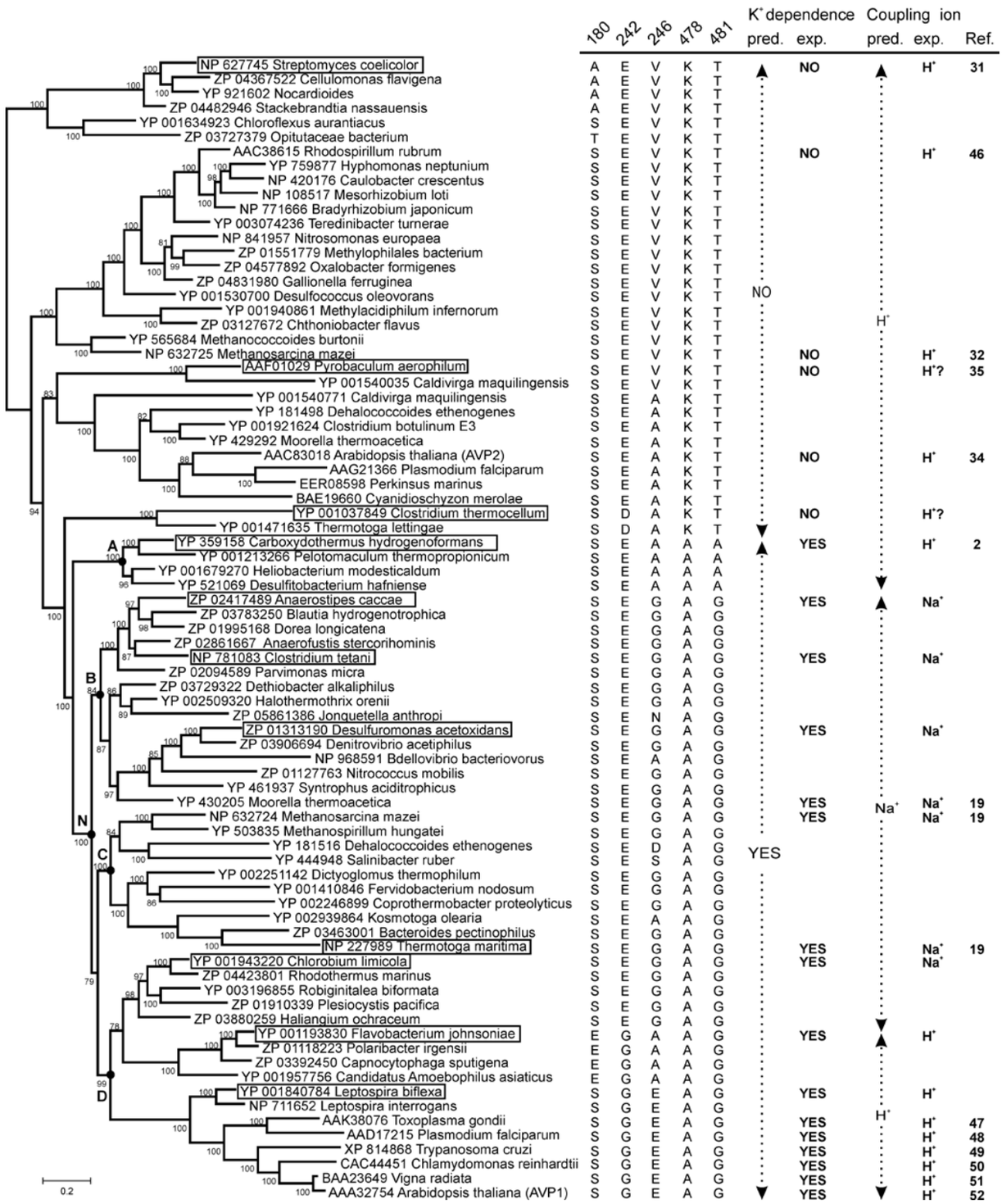
180 242 246 478 481
K+ dependence pred. exp.
Coupling ion pred. exp. Ref.
NP 627745 Streptomyces coelicolor A E V K T NO H+ 31
ZP 04367522 Cellulomonas flavigena A E V K T
YP 921602 Nocardioides A E V K T
ZP 04482946 Stackebrandtia nassauensis A E V K T
YP 001634923 Chloroflexus aurantiacus S E V K T
ZP 03727379 Opitutaceae bacterium T E V K T
AAC38615 Rhodospirillum rubrum S E V K T NO H+ 46
YP 759877 Hyphomonas neptunium S E V K T
NP 420176 Caulobacter crescentus S E V K T
NP 108517 Mesorhizobium loti S E V K T
NP 771666 Bradyrhizobium japonicum S E V K T
YP 003074236 Teredinibacter turnerae S E V K T
NP 841957 Nitrosomonas europaea S E V K T
ZP 01551779 Methylophilales bacterium S E V K T
ZP 04577892 Oxalobacter formigenes S E V K T
ZP 04831980 Gallionella ferruginea S E V K T
YP 001530700 Desulfococcus oleovorans S E V K T NO
YP 001940861 Methylacidiphilum infernorum S E V K T
ZP 03127672 Chthoniobacter flavus S E V K T H+
YP 565684 Methanococcoides burtonii S E V K T
NP 632725 Methanosarcina mazei S E V K T NO H+ 32
AAF01029 Pyrobaculum aerophilum S E V K T NO H+? 35
YP 001540035 Caldivirga maquilingensis S E V K T
YP 001540771 Caldivirga maquilingensis S E A K T
YP 181498 Dehalococcoides ethenogenes S E A K T
YP 001921624 Clostridium botulinum E3 S E A K T
YP 429292 Moorella thermoacetica S E A K T
AAC83018 Arabidopsis thaliana (AVP2) S E A K T NO H+ 34
AAG21366 Plasmodium falciparum S E A K T
EER08598 Perkinsus marinus S E A K T
BAE19660 Cyanidioschyzon merolae S E A K T
YP 001037849 Clostridium thermocellum S D A K T NO H+?
YP 001471635 Thermotoga lettingae S D A K T
A YP 359158 Carboxydothermus hydrogenoformans S E A A A YES H+ 2
YP 001213266 Pelotomaculum thermopropionicum S E A A A
YP 001679270 Heliobacterium modesticaldum S E A A A
YP 521069 Desulfitobacterium hafniense S E A A A
ZP 02417489 Anaerostipes caccae S E G A G YES Na+
ZP 03783250 Blautia hydrogenotrophica S E G A G
ZP 01995168 Dorea longicatena S E G A G
ZP 02861667 Anaerofustis stercorihominis S E G A G
NP 781083 Clostridium tetani S E G A G YES Na+
B ZP 02094589 Parvimonas micra S E G A G
ZP 03729322 Dethiobacter alkaliphilus S E G A G
YP 002509320 Halothermothrix orenii S E G A G
ZP 05861386 Jonquetella anthropi S E N A G
ZP 01313190 Desulfuromonas acetoxidans S E G A G YES Na+
ZP 03906694 Denitrovibrio acetiphilus S E G A G
NP 968591 Bdellovibrio bacteriovorus S E A A G
ZP 01127763 Nitrococcus mobilis S E G A G
YP 461937 Syntrophus aciditrophicus S E G A G
YP 430205 Moorella thermoacetica S E G A G YES Na+ Na+ 19
N NP 632724 Methanosarcina mazei S E G A G YES Na+ 19
YP 503835 Methanospirillum hungatei S E G A G
YP 181516 Dehalococcoides ethenogenes S E D A G
C YP 444948 Salinibacter ruber S E S A G YES
YP 002251142 Dictyoglomus thermophilum S E G A G
YP 001410846 Fervidobacterium nodosum S E G A G
YP 002246899 Coprothermobacter proteolyticus S E G A G
YP 002939864 Kosmotoga olearia S E A A G
ZP 03463001 Bacteroides pectinophilus S E G A G
NP 227989 Thermotoga maritima S E G A G YES Na+ 19
YP 001943220 Chlorobium limicola S E G A G YES Na+
ZP 04423801 Rhodothermus marinus S E G A G
YP 003196855 Robiginitalea biformata S E G A G
ZP 01910339 Plesiocystis pacifica S E G A G
ZP 03880259 Haliangium ochraceum S E G A G
YP 001193830 Flavobacterium johnsoniae E G A A G YES H+
ZP 01118223 Polaribacter irgensii E G A A G
ZP 03392450 Capnocytophaga sputigena E G A A G
YP 001957756 Candidatus Amoebophilus asiaticus E G A A G
D YP 001840784 Leptospira biflexa S G E A G YES H+
NP 711652 Leptospira interrogans S G E A G
AAK38076 Toxoplasma gondii S G E A G YES H+ 47
AAD17215 Plasmodium falciparum S G E A G YES H+ 48
XP 814868 Trypanosoma cruzi S G E A G YES H+ 49
CAC44451 Chlamydomonas reinhardtii S G E A G YES H+ 50
BAA23649 Vigna radiata S G E A G YES H+ 51
AAA32754 Arabidopsis thaliana (AVP1) S G E A G YES H+ 52
0.2

Fig. 2

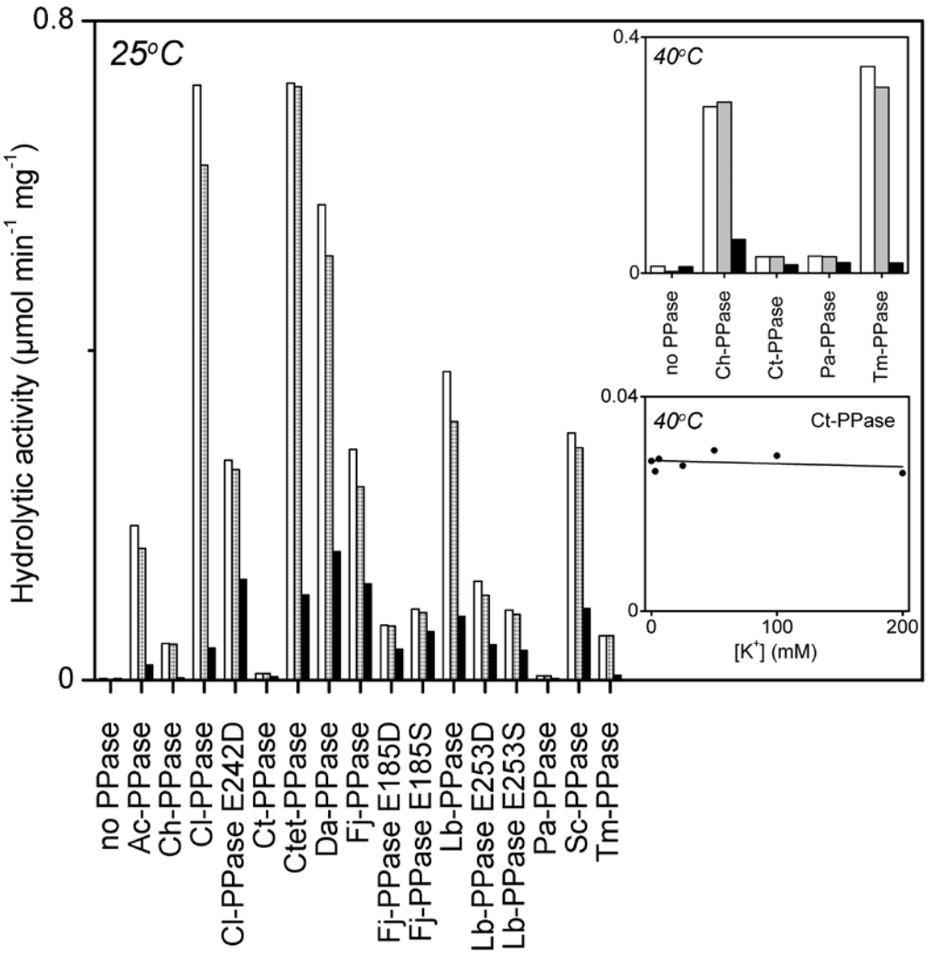
0.8
25°C
Hydrolytic activity (µmol min-1 mg-1)
0
no PPase
Ac-PPase
Ch-PPase
Cl-PPase
Cl-PPase E242D
Ct-PPase
Ctet-PPase
Da-PPase
Fj-PPase
Fj-PPase E185D
Fj-PPase E185S
Lb-PPase
Lb-PPase E253D
Lb-PPase E253S
Pa-PPase
Sc-PPase
Tm-PPase
0.4
40°C
0
no PPase
Ch-PPase
Ct-PPase
Pa-PPase
Tm-PPase
0.04
40°C
Ct-PPase
0
0
100
200
[K+] (mM)

Fig. 3

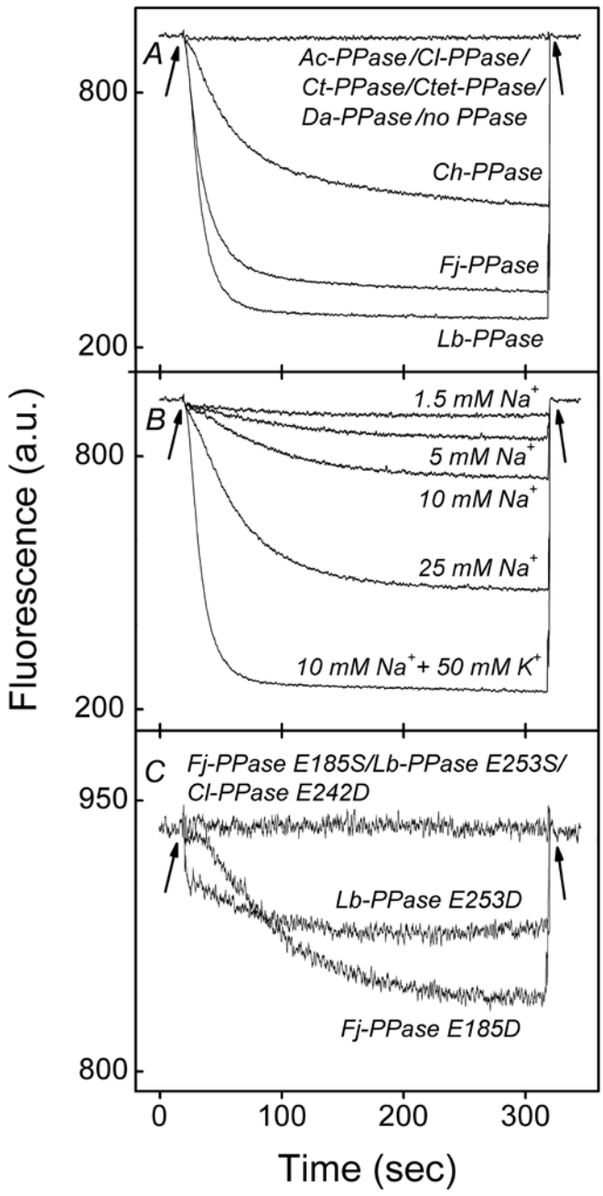
A
Ac-PPase/Cl-PPase/
Ct-PPase/Ctet-PPase/
Da-PPase/no PPase
Ch-PPase
Fj-PPase
Lb-PPase
800
200
B
1.5 mM Na+
5 mM Na+
10 mM Na+
25 mM Na+
10 mM Na+ + 50 mM K+
800
200
C
Fj-PPase E185S/Lb-PPase E253S/
Cl-PPase E242D
Lb-PPase E253D
Fj-PPase E185D
950
800
Fluorescence (a.u.)
0
100
200
300
Time (sec)

Fig. 4

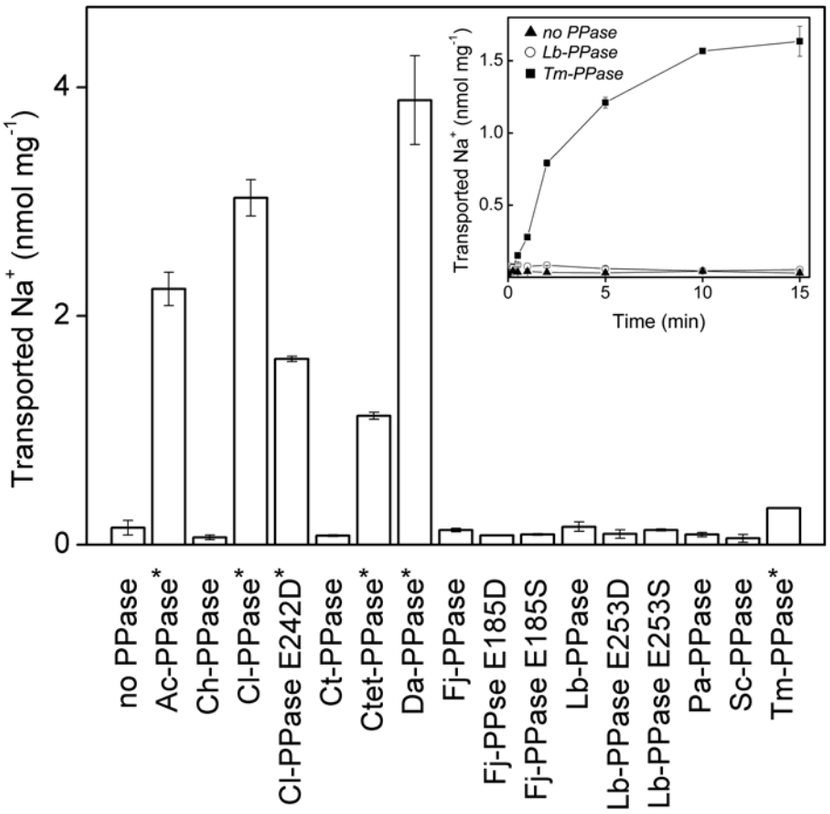
Transported Na+ (nmol mg-1)
0
2
4
no PPase
Ac-PPase*
Ch-PPase
Cl-PPase*
Cl-PPase E242D*
Ct-PPase
Ctet-PPase*
Da-PPase*
Fj-PPase
Fj-PPse E185D
Fj-PPase E185S
Lb-PPase
Lb-PPase E253D
Lb-PPase E253S
Pa-PPase
Sc-PPase
Tm-PPase*
no PPase
Lb-PPase
Tm-PPase
Transported Na+ (nmol mg-1)
0.5
1.0
1.5
0
5
10
15
Time (min)

Fig. 5

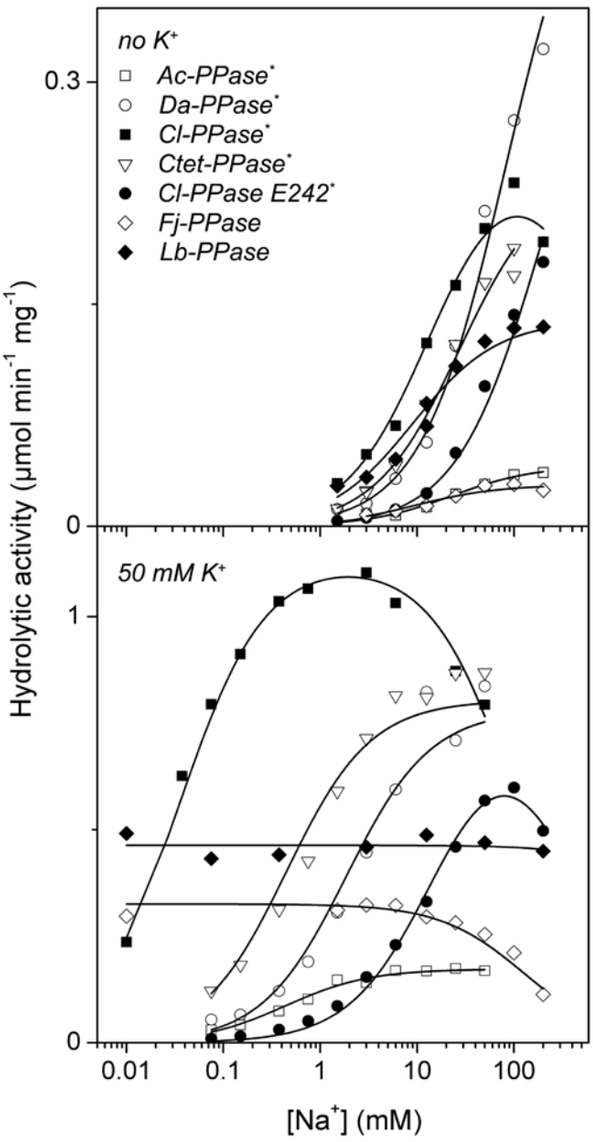
no K+
Ac-PPase*
Da-PPase*
Cl-PPase*
Ctet-PPase*
Cl-PPase E242*
Fj-PPase
Lb-PPase
50 mM K+
Hydrolytic activity (μmol min-1 mg-1)
0.3
0
1
0
0.01
0.1
1
10
100
[Na+] (mM)

Fig. 6

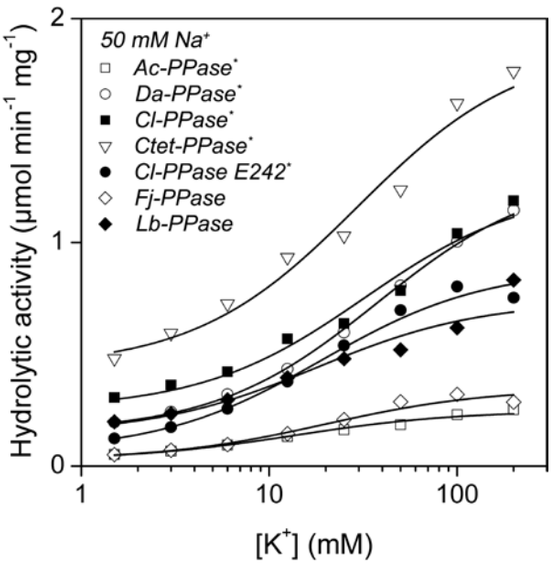
50 mM Na+
Ac-PPase*
Da-PPase*
Cl-PPase*
Ctet-PPase*
Cl-PPase E242*
Fj-PPase
Lb-PPase
Hydrolytic activity (µmol min-1 mg-1)
[K+] (mM)
0
1
2
1
10
100

SUPPLEMENTAL DATA [LUOTO *et al.* (2011)]

Supplementary Table S1
Primers used for cloning and site-directed mutagenesis of membrane PPases

Target enzyme	Primer name	Sequence (5'→3')	Restriction site	Purpose
Ac-PPase	Acac_for	tata*catatg*actaaaagtcataaactcaaattc	NdeI	Cloning
	Acac_rev2	tata*ctcgag*ttataaaattccgccgatact	XhoI	Cloning
Cl-PPase	Clim_for	tata*catatg*aatcaaaccattctctatgc	NdeI	Cloning
	Clim_rev	tata*ctcgag*ttaaagcagcggagcg	XhoI	Cloning
	ClE242S_for	ccgacctttt*tca*agctatgtagg	-	E242S substitution
	ClE242D_for	ccgacctttt*gat*agctatgtagg	-	E242D substitution
	Cl_rev726	cgcccatacccgcaacg	-	Used with ClE242S_for and ClE242D_for
	ClS180E_for	tcggcgca*gag*tccatcg	-	E180S substitution
	ClS180E_rev	gcgagaagccggagataaggttg	-	Used with ClE180S_ for
	Cl_for736	g*c*cgcaatcatcggaac	-	A246G substitution, used with Cl_rev736
	Cl_rev736	tacatagctttcgaaaaggtcgg	-	A246G substitution, used with Cl_for736
Ctet-PPase	Ct_for	tata*catatg*attcagattactacccaa	NdeI	Cloning
	Ct_rev	tata*ctcgag*ttagaaaattgagtacataaggaa	XhoI	Cloning
Da-PPase	Dace_for	tata*catatg*gcatattttgccgtaatt	NdeI	Cloning
	Dace_rev2	tata*ctcgag*ttaggctaacagcggtgc	XhoI	Cloning
Fj-PPase	Fla_full	tata*catatg*aatgcatttatgatttacctg	NdeI	Cloning
	Fla_rev	tata*ctcgag*ttatttagcggcttccactt	XhoI	Cloning
	Fjohn_m553_for	gcttggtgca*tca*tcaattgcttt	-	E185S substitution
	FjE185D_for	gcttggtgca*gat*tcaattgcttt	-	E185D substitution
	Fjohn_m553_rev	gaaaatcccgctaaagtttctaaaacaac	-	Used with Fjohn_m553 _for, FjE185D_for
	F_john_for739	gagctgatttatttt*gaa*tcgtatgtggc	-	G247E substitution
	Fjohn_m739_rev	ccataccggcaacatcacctac	-	Cloning, used with F_john_ for739
Lb-PPase	Lep_for_full	tata*catatg*aatgtagagttaatcattatcgtca	NdeI	Cloning
	Lep_rev_full	tata*ctcgag*ttatttgaagaagtttaaaacaattcc	XhoI	Cloning
	Lep_full_midfor	ccattgat*gcg*tatggtc	-	Elimination of internal NdeI site
	Lep_full_midrev	gaccatacgcatcaatgg	-	Elimination of internal NdeI site
	LbE253D_for	ttctgctgcg*gat*gccacttgt	-	E253D substitution
	LbE253D_rev	ccaaaaaggtcagcacccataccc	-	Cloning, used with LbE253D_ for
	LbE253S_for	ttctgctgcg*tca*gccacttgt	-	E253S substitution
	Lb253rev	ccaaaaaggtcagcacccatacc	-	Used with LbE253S_ for
	Lbif_m745_for	gaagccacttgtgcggcc	-	Used with Lbif_m745 _rev
	Lbif_m745_rev	cgcagcaga*ttc*aaaaaggtcagc	-	G249E substitution
	Lbif_m757_for	*a*tctgctgcg*ggc*gccacttgt	-	E253G substitution, used with Lb253rev. G249E/E253G substitution, used with Lbif_m757_rev
	Lbif_m757_rev	*t*caaaaaggtcagcacccataccc	-	Used with Lbif_m757_ for, part of the G249E

				substitution
Pa-PPase	Ppa_for	tata*catatg*ataagctatgccttactagg	NdeI	Cloning
	Ppa_rev	tata*aagctt*ttagaaaggcaatagacctgacg	HindIII	Cloning
Sc-PPase	Scop_for	ttt*catatg*gcggagcttcctacc	NdeI	Cloning
	Scop_rev	ttt*aagctt*ctacgaaaccacggccg	HindIII	Cloning
Restriction enzyme recognition sites and nucleotide substitutions are underlined and italicized within the primer sequences, respectively.				

Supplementary Figure S1.

Western blots of recombinant membrane PPases in *E. coli* IMV. IMV proteins (3−40 mg/ml) were denatured by incubating for 15 min with an equal volume of SDS loading buffer (139 mM Tris-HCl, pH 6.8, 22% glycerol, 4% SDS, 5 mM DTT and 0.5 mg/ml bromophenol blue) at 50°C, and separated (0.2–2 μg protein) on pre-cast mini SDS-PAGE gels (4–20% acrylamide gradient, Idgel). The electrophoresed samples were transferred to a nitrocellulose membrane (Whatman) in standard Towbin buffer (53) containing 20% (v/v) methanol for 1 h at 100 V in a Mini Trans-Blot apparatus (Bio-Rad). Membrane PPase bands were visualized by Western analysis using rabbit antiserum raised against conserved amino acid motifs in the third cytoplasmic loop of the enzyme (19).

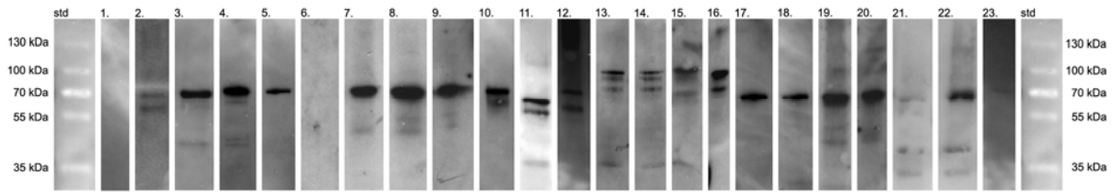

1. no PPase
2. Ac-PPase
3. Ch-PPase
4. Cl-PPase
5. Cl-PPase E242D
6. Cl-PPase E242S
7. Cl-PPase G246A
8. Cl-PPase S180E/E242G
9. Cl-PPase S180E/E242G/G246A
10. Ct-PPase
11. Ctet-PPase
12. Da-PPase
13. Fj-PPase
14. Fj-PPase E185D
15. Fj-PPase E185S
16. Fj-PPase E185S/G247E
17. Lb-PPase
18. Lb-PPase E253D
19. Lb-PPase E253S
20. Lb-PPase G249E/E253G
21. Pa-PPase
22. Sc-PPase
23. Tm-PPase

REFERENCES FOR SUPPLEMENTAL DATA

19. Malinen, A. M., Belogurov, G. A., Baykov, A. A., and Lahti, R. (2007) *Biochemistry* **46**, 8872-8878
53. Towbin, H., Staehelin, T., and Gordon, J. (1979) *Proc Natl Acad Sci U S A* **76**, 4350-4354